A COMBINED RANS-LES STRATEGY WITH ARBITRARY INTERFACE LOCATION FOR NEAR-WALL FLOWS

Lionel Temmerman, Michael A. Leschziner
Department of Aeronautics, Imperial College London,
London SW7 2AZ, United Kingdom
lionel.temmerman@imperial.ac.uk, mike.leschziner@imperial.ac.uk

Kemo Hanjalić
Department of Applied Physics, TU Delft
Lorentzweg 1, 2628 CJ Delft, The Netherlands
hanjalic@ws.tn.tudelft.nl

ABSTRACT

A hybrid RANS-LES methodology is proposed for simulating flows that demand a high-quality resolution of the near-wall region. The method allows the thickness of the near-wall (unsteady) RANS to be chosen freely. This layer is interfaced to the outer LES region subject to compatibility conditions for velocity and turbulent viscosity imposed across the interface. These are extracted dynamically as the simulation progresses. In the RANS layer, one-equation, $k - l$, models are currently used and interfaced to one-equation subgrid-scale models. The effectiveness of the method is examined by reference to fully-developed channel flow at $Re_b = 42000$ and a separated flow in a channel constricted by curved hill-shaped obstructions.

INTRODUCTION

The successful exploitation of large-eddy simulation (LES) for the accurate prediction of wall-bounded flows at high Reynolds numbers is severely constrained by resolution requirements near walls. Grid distances need to be of order $\Delta y^+ = O(1)$, $\Delta x^+ = O(50)$, $\Delta z^+ = O(20)$ to resolve adequately the dynamically influential near-wall structure, which is characterised by progressively smaller scales. In effect, a LES has to approach a Direct Numerical Simulation (DNS) at the wall, with the grid density rising with $Re^{1.8}$ (Chapman, 1979) in comparison with $Re^{0.5}$ away from the wall.

The adoption of near-wall approximations, in conjunction with relatively coarse grids, appears to be the only route to circumventing the above constraints and allowing high-Reynolds-number flows of practical relevance to be simulated at tolerable cost. The essential objective is to provide the option of using a much coarser grid, in all directions or at least parallel to the wall, possibly supplemented by time-saving numerical simplifications in the near-wall region. How to derive and implement such approximations without unacceptable loss of accuracy is an issue of much current concern.

Two principal strategies have been proposed: the first involves the use of log-law-based wall functions (Deardorff, 1970; Schumann, 1975; Werner and Wengle, 1991; Hoffman and Benocci, 1995) to bridge the viscous sub-layer, as has been done for many years in Reynolds-Averaged Navier-Stokes (RANS) calculations performed with 'high-Reynolds-number' turbulence models. The other, more recent strategy is based on combining RANS-type representations of the near-wall flow with a LES solution in the outer flow (or, in rare cases, vice versa). This hybridisation poses a whole raft of fundamental and practical problems. One question is how to reconcile the high degree of unsteadiness induced by the simulation in the near-wall layer with the concept of time-averaging and the closure approximations underpinning the RANS approach. Apart from the fundamental facet of this question, there is the practical issue of how to avoid 'double-counting' of turbulence in the unsteady RANS layer and how to achieve continuity across the RANS-LES 'interface'.

The *Detached Eddy Simulation* (DES) strategy of Spalart et al. (1997) is the best-known RANS-LES combination. A single one-equation model (Spalart and Allmaras, 1992) is used for both RANS and LES regions, together with the interface condition $y_{int} = \min(y, C_{DES}\max(\Delta x, \Delta y, \Delta z))$, where y is the wall distance. A related proposal is the *Limited Numerical Scales* (LNS) formulation of Batten et al. (2001), wherein the switch is effected upon a comparison of the eddy-viscosity values returned by the RANS model and subgrid-scale (SGS) models used, the smaller taking precedence. Another approach, the *Thin Boundary Layer Method* (TBL) (Balaras and Benocci, 1994; Balaras et al., 1996; Cabot and Moin, 1999), entails the solution, within a specified wall layer, of the thin-shear-flow forms of the Navier-Stokes (NS) equations, which then provide an unsteady boundary condition in the form of the wall shear stress or wall-parallel velocity to the LES region. Finally, *zonal* hybrid approaches have been pursued by Davidson and Peng (2001), Hamba (2001), Temmerman et al. (2002). In these, the interface location is freely chosen, both zones are solved in a numerically identical unsteady manner, and each zone provides the other with unsteady interface conditions, subject to certain constraints and modifications. The nature of these conditions, and the manner in which they ensure compatibility between the two zones is here the key issue. One practice, pursued by Quéméré and Sagaut (2002), involves a reconstruction of the spectral content of the interface conditions from the statistical RANS properties to provide unsteady conditions to the LES zone.

The present paper investigates a URANS-LES method which is of the *zonal* type. It allows the interface to be chosen freely, in principle. A particular focus is the manner in which the two regions are coupled. The main features of

the methodology and the models employed are presented, and the performance of the method is then illustrated by reference to simulations for channel and separated flows.

PRINCIPAL LESSONS DERIVED FROM A-PRIORI TESTS

In an earlier paper, Temmerman et al. (2002) have investigated the response of the turbulence properties in a RANS near-wall layer of a channel flow to the imposition of the LES solution, obtained in parallel, at the edge of the layer, with the LES being unaffected of the layer, and the layer treated by a thin-shear-flow numerical approximation. Tests were conducted for a periodic turbulent channel flow at a Reynolds number, based on bulk velocity and channel half-width, of 10935 and a layer thickness $y^+ = 65$. An important observation made in this study was that the resolved motion in the RANS region was not materially weaker than that in the overlapping LES region; this is illustrated by Fig. 1. Moreover, the correlation, in terms of magnitude and direction, between the wall shear stress and wall-parallel velocity at different y^+ values was similar in both RANS and LES region. Hence, the resolved contribution to statistical turbulence properties was substantial. At the same time, the RANS model - in that particular case, the one-equation turbulence-energy model of Wolfshtein (1969) - also returned a substantial contribution. Thus, as shown in Fig. 2, the sum of modelled and resolved components of the turbulence energy in the RANS region was significantly larger than the real value, based on DNS data and returned by the LES. At the interface, a discontinuity results, with the resolved and modelled components obtained from the RANS region observed to be significantly different from their LES counterparts, leading to the conclusion that compatibility constraints were needed in order to couple the two regions in any fully interactive simulation. This aspect was further illustrated by the substantial difference of magnitude between the LES and RANS modelled viscosities far away from the wall (Fig. 2).

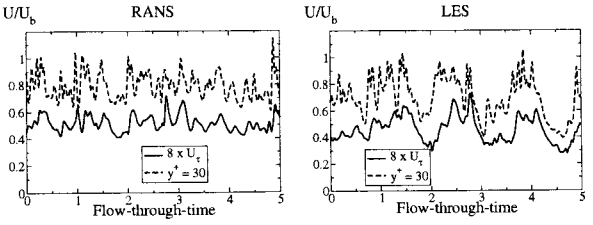

Figure 1: Time history for the velocity ($y^+ = 30$) and wall-shear velocity for the a-priori RANS and the equivalent LES.

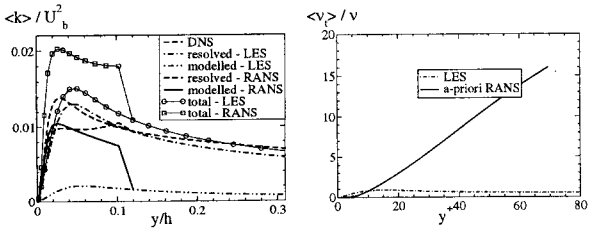

Figure 2: Turbulence-energy and modelled turbulent viscosity profiles for the a-priori RANS and the equivalent LES in comparison to DNS.

METHODOLOGY

Both RANS and LES zones are solved using the same numerical methodology, which is based on a co-located storage, second-order centred finite-volume approach and a second-order fractional-step projection method in which the pressure equation is solved by using a partial diagonalisation in combination with a multigrid algorithm (see Temmerman et al. (2003)).

In the present work, one-equation models for the transport of the modelled turbulence energy are considered, both in the RANS and LES regions:

$$\frac{\partial k}{\partial t} + \frac{\partial \left(U_j k\right)}{\partial x_j} = P + \frac{\partial}{\partial x_j}\left[\left(\nu + \frac{\nu_t}{\sigma_k}\right)\frac{\partial k}{\partial x_j}\right] - \epsilon \qquad (1)$$

in which all dependant quantities are associated either with phase-average motion in the URANS region or SGS motion in the LES region. The differences between the RANS and SGS models lie in the way the dissipation and the turbulent viscosity are defined. In the present study, the SGS model is that of Yoshizawa and Horiuti (1985), wherein:

$$\epsilon = \frac{k^{1.5}}{C_\Delta \Delta} \quad , \quad \nu_t = C_\mu \frac{k^2}{\epsilon}$$
$$C_\mu = 0.09 \quad , \quad C_\Delta = 0.61 \quad , \quad \Delta = \left(\Delta x \Delta y \Delta z\right)^{\frac{1}{3}} \qquad (2)$$

The RANS models used here are those of Wolfshtein (1969) and, alternatively, of Norris and Reynolds (1975). The Wolfshtein model is:

$$\epsilon = \frac{k^{1.5}}{l_\epsilon}, \quad \nu_t = C_\mu l_\mu k^{0.5}, \quad l_\mu = C_l y\left(1 - exp\left(-0.016 y^*\right)\right)$$
$$l_\epsilon = C_l y\left(1 - exp\left(-0.263 y^*\right)\right), \quad y^* = \frac{y k^{0.5}}{\nu}$$
$$C_\mu = 0.09, \quad C_l = \kappa C_\mu^{-0.75}, \quad \kappa = 0.41 \qquad (3)$$

where y is the distance to the nearest wall. The Norris-Reynolds model differs from the Wolfshtein form in respect of the characteristic length-scales l_ϵ and l_μ:

$$l_\mu = \kappa y\left(1 - exp\left(-0.0198 y^*\right)\right), \quad l_\epsilon = \kappa y \frac{y^*}{y^* + 2\kappa C_\mu^{-0.75}} \qquad (4)$$

At the interface, the RANS and LES zones interchange velocities, turbulent viscosity and modelled turbulence energy as indicated schematically in Fig. 3. Based on the observations of the *a-priori* tests discussed earlier, cross-interface compatibility is required, and the present proposal is to enforce continuity in the total viscosity across the interface:

$$\nu_{LES}^{mod} + \nu_{LES}^{res} = \nu_{RANS}^{mod} + \nu_{RANS}^{res} \qquad (5)$$

where the resolved LES viscosity may be extracted from:

$$\nu_{LES}^{res} = \frac{\left(\overline{u_i}'\,\overline{u_j}' - \overline{u_k}'\,\overline{u_k}'\delta_{ij}/3\right)\overline{S_{ij}}}{\overline{S_{ij}}\,\overline{S_{ij}}} \qquad (6)$$

with the overbar identifying filtered quantities and primes denoting turbulent fluctuations. On the RANS side, the total viscosity is the sum of modelled turbulent viscosity and the resolved component ν_{RANS}^{res} which may be evaluated in a manner analogous to (6). Because the resolved stresses are required to be continuous across the interface, Eqs. (5) and (6) imply, at the interface:

$$\nu_{LES}^{mod} = \nu_{RANS}^{mod} \qquad (7)$$

Assuming, for the sake of argument, that a k-ϵ model is used in the RANS layer,

$$\nu_{RANS}^{mod} = C_\mu f_\mu \frac{k_{RANS}^{mod\,2}}{\epsilon_{RANS}^{mod}} \qquad (8)$$

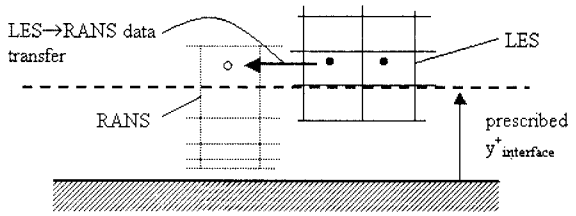

Figure 3: Two-layer (RANS-LES) near-wall region.

The constraint expressed by Eq. (5) can be imposed by the modification:

$$C_\mu = \frac{< \nu^{mod}_{LES}/\epsilon^{mod}_{RANS} >}{< f_\mu k^{mod\,2}_{RANS}/\epsilon^{mod}_{RANS} >} \qquad (9)$$

where $\langle\cdot\rangle$ is a local averaging operator such as spatial averaging in homogeneous directions. The coefficient C_μ is extracted at the interface from relation (9) and is then adapted so as to increase the modelled contribution of the RANS model as the wall is approached. Two possible variations have been explored:

$$C_\mu(y) = 0.09 + (C_{\mu,int} - 0.09)\,\frac{(1 - exp(-y/\Delta))}{(1 - exp(-y_{int}/\Delta_{int})} \qquad (10)$$

and

$$\begin{cases} C_\mu(y) = 0.09\frac{y^+}{27} & \text{for} \quad y^+ \le 27 \\ C_\mu(y) = 0.09 + \frac{(C_{\mu,int}-0.09)(1-exp(-(y-y(y^+=34))/\Delta))}{(1-exp(-(y_{int}-y(y^+=34))/\Delta_{int})} \\ \text{for} \quad y^+ > 27 \end{cases} \qquad (11)$$

where y is the distance from the wall, the subscript 'int' identifies the interface, $\Delta = (\Delta x \Delta y \Delta z)^{1/3}$ and $C_{\mu,int}$ is obtained from (9). The choice of (11) is based on the observed near-wall variation of C_μ extracted from $\nu_t = C_\mu f_\mu k^2/\epsilon$ where k, ϵ and $\nu_t = - < u'v' > /\partial u/\partial y$ extracted from DNS data for turbulent channel flow by Moser et al. (1999). The coefficient is observed to be close to 0.09 outside the buffer layer, decreasing roughly linearly up to $y^+ = 5$.

RESULTS

Channel flow at high Reynolds number

The performance of the present LES-RANS scheme is first assessed for a turbulent channel flow at a half-channel-width Reynolds number of 42200. Several other channel flows, at lower Reynolds numbers, have also been examined. The computations undertaken are summarised in Table 1, and related solutions are presented in Figs. 4-8. The table also lists the modelling practices adopted and location of the interface of the RANS and LES zones in terms of wall coordinates. All hybrid RANS-LES simulations were performed on a domain size of $2\pi h \times 2h \times \pi h$, covered with $64 \times 64 \times 32$ cells, the 32 cells extending over the spanwise extent. The cell dimensions are $\Delta x^+ = \Delta z^+ = 196$ and $\Delta y^+ = 0.8 - 222$, the value 0.8 pertaining to the near-wall cell, and 222 to the channel centre. In agreement with a recommendation by Shur et al. (1999), the cells have an aspect ratio $\Delta x^+/\Delta z^+ = 1$. The hybrid-scheme solutions are compared to a LES computation (denoted LES) performed on that grid, and to a highly resolved LES computation (denoted LES ref.) on a domain of $2\pi h \times 2h \times \pi h/2$ covered by $512 \times 128 \times 128$ cells of size $\Delta x^+ = \Delta z^+ = 24.5$ and $\Delta y^+ = 1.5 - 86$. Experimental data of Wei and Willmarth (1998) (denoted WW) at a similar Reynolds number are also used below for comparison. Both LES computations used the WALE sgs model of Nicoud and Ducros (1999).

Table 1: Description of the channel cases. Abbreviations: n.a., not applicable; Y., Yoshizawa; W., Wolfshtein; NR., Norris & Reynolds; int, interface.

Case	LES Model	RANS Model	C_μ	y^+_{int}
LES ref.	WALE	n.a.	n.a.	n.a.
LES coarse	WALE	n.a.	n.a.	n.a.
C1	Y.	W.	(9) & (10)	48
C2	Y.	W.	(9) & (10)	135
C3	Y.	W.	(9) & (11)	135
C4	Y.	W.	(9) & (11)	318
C5	Y.	NR.	(9) & (11)	135

Fig. 4 shows the distribution of C_μ for cases C1 to C5. The C_μ value at the interface is seen to be of the order 0.01-0.04. This reflects the low level of sgs viscosity relative to that the RANS model would generate. In C1 relative to C2, the interface location has been shifted from $y^+ = 135$ to $y^+ = 48$, and the C_μ interface value computed for the latter is seen to fall onto the distribution prescribed by relation(10) for the former. Hence, the similarity of the solutions for these two cases is not surprising. This behaviour, while encouraging in implying a weak dependence on the location of the interface when relation (10) is used, is not general and reflects the particular near-wall SGS viscosity variation returned by the Yoshizawa-Horiuti model used in the computation. This is recognised upon comparing cases C3, C4 and C5 in Fig. 4, the interface in C4 being placed at the high value of $y^+ = 318$. Case C5 uses the Norris-Reynolds model, while case C3 was computed with the Wolfshtein model. However, the differences arising from the change in model are observed to be insignificant.

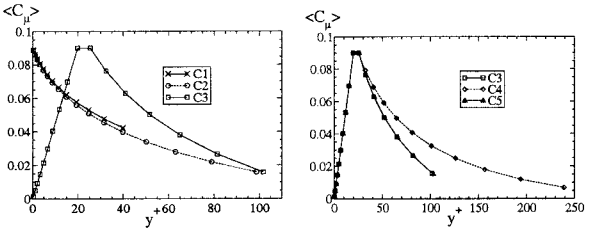

Figure 4: Time-averaged C_μ profiles across the RANS layer for the different cases.

The velocity profile obtained from the coarse-grid LES on the same grid as the hybrid computations differs dramatically from the reference LES computation, performed on a $512 \times 128 \times 128$ cells grid. The latter adheres well to the experimental results of Wei and Willmarth (1998) (denoted WW in the figures) and thus represents a credible reference solution. The RANS-LES computations (cases C1 to C5) yield much better results, though they imply somewhat excessive levels of viscosity around the interface, leading to the observed distortion in the log-law region close to the interface. Changing the RANS model, interface locations and C_μ distribution does not result in substantial changes in the velocity distributions.

The shear-stress plots contain separate profiles for the modelled and resolved contributions. The former rise steeply as the interface is traversed, thus indicating that the RANS model provides the lion's share of the turbulent stress as the wall is approached. As is the case with velocity, the shear

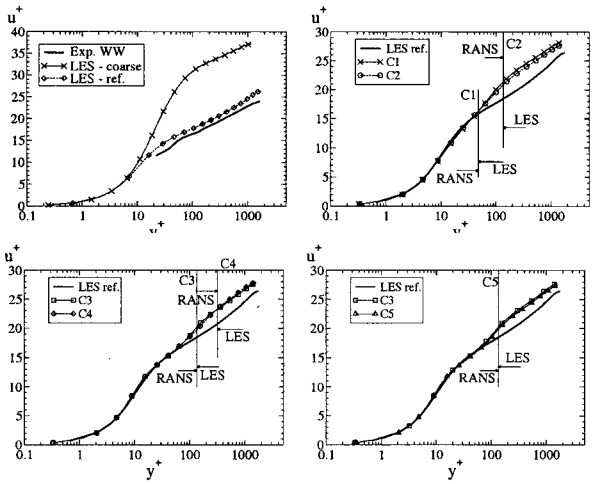

Figure 5: Time-averaged velocity profiles for the different cases.

stress is not greatly influenced either by the C_μ distribution (cases C2 and C3) or by the interface location (cases C3 and C4). In contrast, the turbulence energy is considerably more sensitive to the details of the hybrid strategy. Fig. 7 again distinguishes between the modelled and resolved contributions and also provides profiles of the total energy. Despite the dynamic adjustment, the total turbulence level is too high, especially in the turbulent region just above the buffer layer. This is seen most clearly when comparing cases C3 and C4. The implication is that the resolved contribution remains high in the RANS region close to the interface, resulting in some 'double-counting' of turbulence, despite the low level of C_μ in this region. While the C_μ distribution does not greatly affect the behaviour of the near-wall total turbulence energy, the outward displacement of the interface leads to a progressive thickening of the layer of high turbulence energy, a behaviour consistent with the distortion in velocity in the log-law region noted earlier. Notwithstanding these defects, the level of turbulence energy in the inner LES region is well predicted in all cases. As expected, the modelled turbulent viscosity, shown in Fig. 8, is very sensitive to the location of the interface. It is observed first that the profiles remain continuous across the interface. Previous computations (see Temmerman et al. (2002)) have shown that a discontinuity in the viscosity lead to corresponding discontinuities in the other quantities. As the interface is shifted away from the wall (cases C1 to C2, C3 to C4), the viscosity magnitude raises. The change in the C_μ distribution (cases C2 and C3) is also seen to affect the profile shapes.

The results shown above, although certainly not perfect, may be claimed to be encouraging. The influence of the parameters tested is small, Except for the (desirable) response to changes in the interface location, which affects the proportion of the flow being modelled as well as the width of the near-wall total turbulence energy peak.

Separated flow

The hybrid RANS-LES approach is applied next to the case of a channel with periodically arranged hill-shaped constrictions along one wall, causing massive separation at the leeward side of the constrictions. The computational domain extends from one hill crest to the next (see Fig. 9) with periodic conditions applied at both ends. The Reynolds number, based on the flow rate and the channel height, is 21560. This is a rather low value, making this flow a less than ideal test

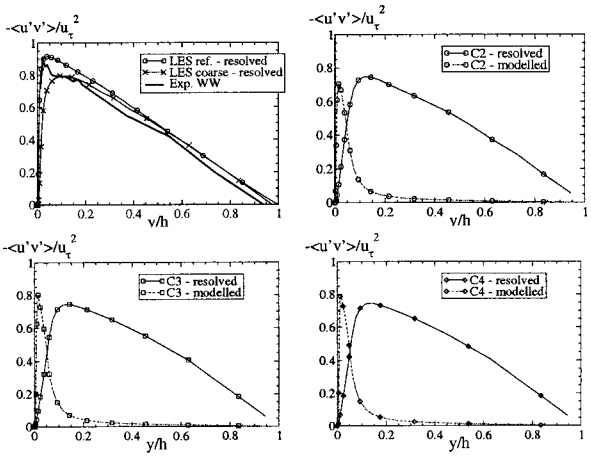

Figure 6: Shear-stress profiles for the different cases.

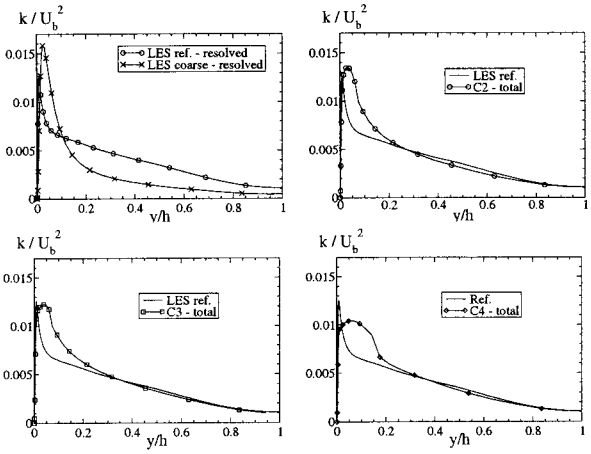

Figure 7: Turbulence energy profiles for the different cases.

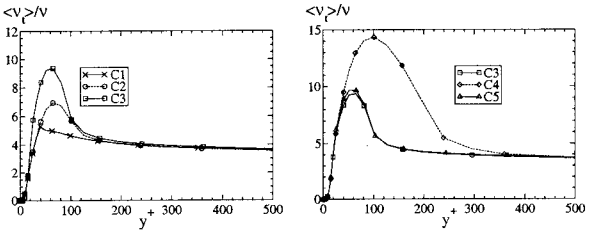

Figure 8: Time-averaged ν_t/ν profiles for the different cases.

case for present purposes.

An extensive study of this flow, with particular emphasis on the sensitivity to wall functions and SGS models, is reported in Temmerman et al. (2003). The availability of extensive data[1] from two highly-resolved simulations over a grid of about 5 million nodes ($196\times128\times186$ cells) allows the accuracy of the present LES-RANS method to be assessed.

A total of seven simulations are compared, Table 2: the highly-resolved reference computation, a LES computation on a coarse grid, a DES computation and four RANS-LES simulations. These five 'coarse-grid' simulations used a wall-resolving grid in *wall-normal direction*, with the centre of the wall-nearest cell located at $y_c^+(1) = O(1)$). This grid, contains $112 \times 64 \times 56 = 4 \cdot 10^5$ cells on a domain size of $9h \times 3.036h \times 4.5h$, with h being the hill height. The resolution of the grid in the streamwise direction is equivalent to the streamwise resolution of the coarsest grid used in Temmerman et al. (2003) for the study of wall-functions. The spanwise resolution was chosen to keep the ratio $\Delta x^+/\Delta z^+$

[1] http://cfd.me.umist.ac.uk/ercoftac/

Table 2: Description of the hill cases. Abbreviations: n.a., not applicable; Y., Yoshizawa; W., Wolfshtein; NR., Norris & Reynolds; SA., Spalart & Allmaras; int, interface.

Case	LES Model	RANS Model	C_μ	j_{int}
Ref.	WALE	n.a.	n.a.	n.a.
LES	WALE	n.a.	n.a.	n.a.
DES	SA.	SA.	n.a.	n.a.
CH1	Y.	W.	(9) & (10)	$j = 13$
CH2	Y.	W.	(9) & (10)	$j = 5$
CH3	Y.	W.	(9) & (10)	$j = 9$
CH4	Y.	NR.	(9) & (10)	$j = 13$

as close to 1 as possible, and this thus gives a much coarser grid than the one used in the reference computation.

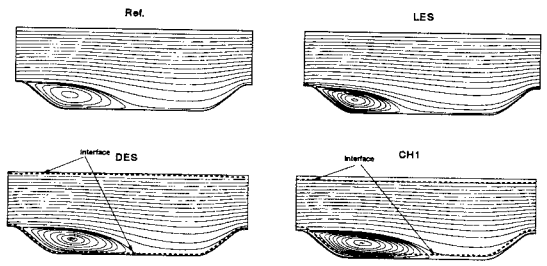

Figure 9: Streamlines for the reference simulation, the LES computation, the DES CH1 cases.

Fig. 9 shows mean streamfunction contours for the reference LES, the coarse-grid LES, the DES and the first hybrid RANS-LES case (CH1). The interface positions are indicated by the dashed lines. In the case of the DES, switching between the RANS and LES zone is controlled by the grid, and this occurs here at around the very low value of $y^+ = 5 - 10$. In contrast, the interface value for CH1 is of order $y^+ = 20 - 100$, depending on the streamwise position (see Fig. 10). A significantly higher value of y^+ would placed the interface too close to the centre of the recirculation zone, a choice found to give an aberrant behaviour. The reference and coarse-grid LES computations yield similar recirculation zones. This observation is confirmed in Table 3, which gives the locations of the separation and reattachment points in terms of the streamwise location x/h. In contrast, the recirculation zones predicted by both DES and the hybrid RANS-LES computations are too long. The separation point is predicted correctly by all RANS-LES computations, but this feature depends primarily on the grid resolution around the separation point (Temmerman et al., 2003). Switching from the Wolfshtein to the Norris-Reynolds model (compare cases CH1 and CH4) leads to a minor reduction in the length of the recirculation zone. A test, in which the wall shear-stress-stress distribution generated by the LES was imposed (in a time-accurate fashion) on one of the RANS-LES computations, yielded a recirculation region close to that of the reference LES. This suggests that the primary reason for the undesirable elongation of the recirculation zone returned by the RANS-LES computations is rooted in defects in the wall shear stress predicted by the RANS model.

Fig. 10 shows the location (expressed in wall units) of the interface near the lower wall for cases CH1, CH2 and CH4. In Fig. 11, the $< C_\mu >$ coefficient along the lower interface is plotted against the streamwise location. As was the case in the channel-flow simulation, a substantial reduction in the magnitude of $< C_\mu >$ results as the interface is shifted away from the wall (Fig. 12).

Table 3: Description of the hill cases. Abbreviations: n.a., not applicable; int., interface; loc., location; sep., separation; reat., reattachment.

Case	$(x/h)_{sep.}$	$(x/h)_{reat.}$
Ref.	0.22	4.72
LES	0.23	4.64
DES	0.21	5.30
CH1	0.23	5.76
CH2	0.23	5.43
CH3	0.23	5.65
CH4	0.24	5.52

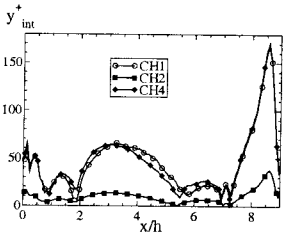

Figure 10: Location of the interface near the lower wall for DES and the RANS-LES case.

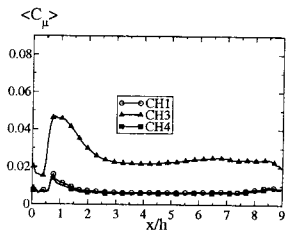

Figure 11: $< C_\mu >$ distribution along the interface.

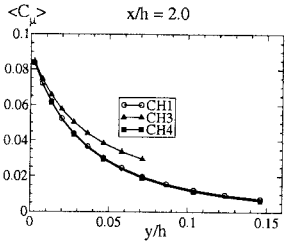

Figure 12: $\langle C_{\mu,dyn} \rangle$ distribution in the vertical direction in the lower RANS region.

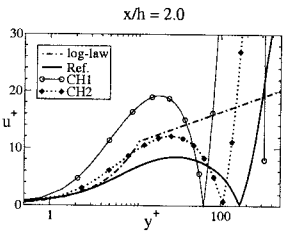

Figure 13: Velocity profiles expressed in wall units for the lower RANS region at one streamwise locations.

Streamwise velocity profiles, in wall units, at $x/h = 2$ are shown in Fig. 13 for CH1 and CH2 in comparison with the log-law and the profile arising from the reference simulation. Velocity profiles derived from all computations at two streamwise positions are included in Fig. 14. One message conveyed by the former figure is that the near-wall velocity is very far from the log-law. Thus, the use of wall functions in this region is not a credible practice. While there are clearly differences between the simulated profiles - partly associated with the differences in the size of the recirculation zone and in the wall shear stress - the shape resulting from the RANS-LES simulation is similar to the reference solution. Fig. 13. Also, the actual velocity profiles returned by the RANS-LES computation, Fig. 14, agree reasonably well with the corresponding reference solutions.

Finally, Fig. 15 shows turbulent viscosity profiles for all computations performed on the coarse grid. The viscosity levels resulting from all CH simulations are very similar. The differences relative to the LES and the DES distributions are rooted, principally, in the fact that the SGS models used are different - WALE in the case of the LES computation and the Spalart-Allmaras model in the case of DES. In contrast to the channel-flow computation, the modelled near-wall viscosity is low - indeed, lower than the SGS viscosity in the inner region. This is a consequence of the low Reynolds number of the flow, which, as noted earlier, makes

this case a less than ideal test of the hybrid method.

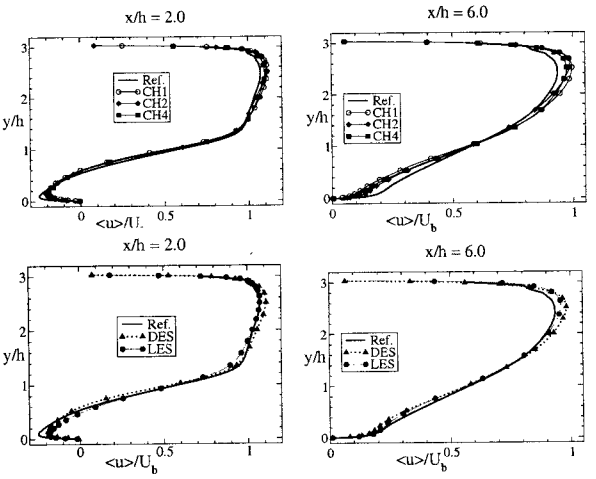

Figure 14: Streamwise velocity profiles at two streamwise locations.

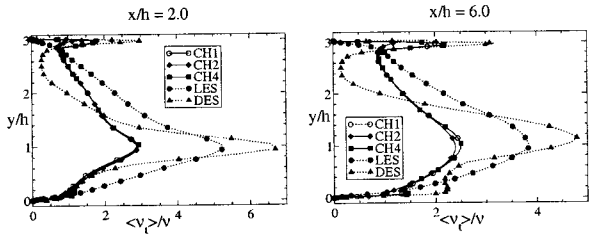

Figure 15: Modelled viscosity at two streamwise locations.

CONCLUSIONS

The principles of a new method linking LES to a RANS-type near-wall treatment have been presented. Major features of the method include: freedom in choosing the location of the interface; a dynamic adjustment of the RANS model at the RANS-LES interface by reference to the subgrid-scale viscosity on the LES side of the interface, designed to secure continuity of modelled viscosity; and a 'relaxation' function steering the modelled viscosity from its interface value to the standard-model value as the wall is approached. While the nature of this function is somewhat arbitrary, it is demonstrated that the interface values extracted from simulations with different RANS-layer thickness adhere, broadly, to the variation which is represented by one of two functional proposals examined in the paper.

In the case of high-Reynolds-number channel flow, the method has been demonstrated to return a behaviour which, while not perfect, is dramatically better than LES on the same coarse grid. The effectiveness of the method is shown to be only weakly dependent on the interface location. The application of the method to a single recirculating flow is somewhat inconclusive, primarily because the relatively low Reynolds number of the flow, for which highly resolved LES data are available, constrained the choice of an appropriately coarse grid which would challenge the method and would be expected to yield poor results for pure LES computations on that grid. For this flow, the LES-RANS method results in an excessively long recirculation zone, and this seems to stem from defects in the wall-shear stress returned by the RANS model.

ACKNOWLEDGMENTS

The authors are grateful to the UK Engineering and Physical Sciences Research Council for supporting the research reported herein.

REFERENCES

Balaras, E., and Benocci, C., 1994, *Proceedings, 74th Fluid Dynamic Symp. on Applications of Direct and Large Eddy Simulation*, Crete, Greece, pp. 2-1 – 2-6.

Batten, P., Goldberg, U.C., Palaniswamy, S., and Chakravarthy, S.R., 2001, *Proceedings, 2nd International Symposium on Turbulence and Shear Flow Phenomena*, Lindborg, E. et al, ed., KTR, Stockholm, Sweden, Vol. 2,pp. 159–164.

Balaras, E., Benocci, C., and Piomelli, U., 1996, *AIAA J.*, Vol. 34, pp. 1111–1119.

Cabot, W., and Moin, P., 1999, *Flow, Turbulence and Combustion*, Vol. 63, pp. 269–291.

Chapman, D.R., 1979,*AIAA J.*, Vol. 17, pp. 1293–1313.

Davidson, L., and Peng, S.-H., 2001,*Proceedings, 2nd International Symposium on Turbulence and Shear Flow Phenomena*, Lindborg, E. et al, ed., KTR, Stockholm, Sweden, Vol. 2, pp. 175–180.

Deardorff, J.W., 1970, *J. Fl. Mech.*, Vol. 61, pp. 481–507.

Hamba, F., 2001,*Theoret. Comput. Fluid Dynamics*, Vol. 14, pp. 323–336

Hoffman, G., and Benocci, C., 1995,*Proceedings, Advances in Turbulence V*, Benzi, R., ed., Kluwer Academic Publishers, pp. 222–228.

Moser, R.D., Kim, J., and Mansour, N.N., 1999, *Phys. Fl.*, Vol. 11, pp. 943–945.

Nicoud, F., and Ducros, F., 1999, *Flow, Turbulence and Combustion*, Vol. 62, pp. 183–200.

Norris, L.H., and Reynolds, W.C., 1975, Rep. F-M10, Dept. of Mech. Eng., Stanford University.

Quéméré, P., and Sagaut, P., 2002, *Int. J. Numer. Methods Fluids*, Vol. 40, pp. 903–926.

Schumann, U., 1975, *J. Comp. Phys.*, Vol. 18, pp. 376–404.

Shur, M., Spalart, P.R., Strelets, M., and Travin, A., 1999, *Proceedings, Engineering Turbulence Modelling and Experiments - 4*, Rodi, W., and Laurence, D., ed., Elsevier Science, Corsica, France, pp. 669–678.

Spalart, P.R., and Allmaras, S.R., 1992, *AIAA Paper 92-0439.*

Spalart, P.R., Jou, W-H., Strelets, M., Allmaras, S.R., 1997, *Proceedings, Advances in DNS/LES, 1st AFOSR Int. Conf. on DNS/LES*, Greden Press.

Temmerman, L., Leschziner, M.A., Mellen, C.P., and Fröhlich, J., 2003, *Int. J. Heat and Fluid Flow*, Vol. 24, pp. 157–180.

Temmerman, L., Leschziner, M.A., and Hanjalić, K., 2002, *Proceedings, 5th Symp. on Engineering Turbulence Modelling and Measurements*, Rodi, W. , and Fueyo, N., ed., Elsevier Science, Maiorca, Spain, pp. 317–326.

Werner, H., and Wengle, H., 1991, *Proceedings, 8th Symp. on Turb. Shear Flows*, pp. 155–168.

Wolfshtein, M., 1969, *Int. J. Heat Mass Transfer*, Vol. 12, pp. 301–318.

Wei, T., and Willmarth, W.W., 1998, *AGARD-AR-345*, AGARD, pp. 122.

Yoshizawa, A., and Horiuti, K., 1985, *J. Phys. Soc. Japan*, Vol. 54, pp. 2834–2839.